Build Simul (2021) 14: 1757–1771
https://doi.org/10.1007/s12273-021-0783-x

Model-based adaptive controller for personalized ventilation and thermal comfort in naturally ventilated spaces

Dalia Ghaddar[1], Mariam Itani[1,2], Nesreen Ghaddar[1] (✉), Kamel Ghali[1], Joseph Zeaiter[3]

1. Mechanical Engineering Department, American University of Beirut, P.O. Box 11-0236, Beirut 1107-2020, Lebanon
2. Mechanical Engineering Department, Phoenicia University, District of Zahrani, Lebanon
3. Bahaa and Walid Bassatne Department of Chemical Engineering and Advanced Energy, American University of Beirut, Beirut, Lebanon

Abstract

This work develops a standalone autonomously controlled personalized ventilation (PV) unit in a naturally ventilated (NV) office space to maintain acceptable thermal comfort (*TC*) under steady and transient indoor conditions and activity levels. The NV-PV proportional integral derivative (PID) controller adjusts the PV supply temperature (T_{SPV}) at the occupant set flow rate (Q_{SPV}) based on predicted *TC* using a regression model. The target *TC* level that the controller attains at all times is between 0 (neutral) and 1 (slightly comfortable). Process transfer functions were developed and then used to find the adaptive PID tuning coefficients using the Internal Model Control (IMC) method. The controller was tested in a case study at indoor temperature range of 25 to 33 °C with relative humidity range of 55% and 80%. It was shown that the NV-PV controller adjusted T_{SPV} to maintain acceptable *TC* under transients of indoor conditions and metabolic rates.

Keywords

adaptive PID controller;
personalized ventilation;
natural ventilation;
thermal comfort

Article History

Received: 31 October 2020
Revised: 02 February 2021
Accepted: 13 February 2021

1 Introduction

Heating, ventilation and air conditioning (HVAC) systems in buildings account for 48% of annual energy consumption in the United States to maintain acceptable indoor environments that provide thermal comfort (*TC*) and good air quality for occupants (Pérez-Lombard et al. 2008; Jazizadeh and Jung 2018). In Europe, around 40% of the energy consumption is attributed to commercial and residential buildings (Pérez-Lombard et al. 2008). However, a recent study on *TC* showed that only 11% of 215 studied office buildings in the United States, Canada, and Finland equipped with HVAC systems were able to ensure comfortable occupant states (Huizenga et al. 2006). To generate an effective indoor thermal environment for occupants, the ventilation system should respond to their *TC* preferences by performing adjustments to its operational settings (Shan et al. 2020). Apart from comfort, conventional HVAC systems consume high amounts of energy as they tend to condition the indoor space's whole volume. However, there is great potential for significant reductions in energy consumption of HVAC systems to attain sustainability goals in indoor environments, as experimentally found by Feldmeier and Paradiso (2010) and Jazizadeh and Jung (2018).

In moderate climates, natural ventilation (NV) is one of the most effective sustainable strategies for energy savings related to building usage while assuring the supply of adequate breathing air and acceptable ventilation of contaminants (Yang and Clements-Croome 2012; Nomura and Hiyama 2017). However, the success of NV in providing *TC* for the occupants relies on outdoor temperature and indoor loads. At the elevated indoor conditions above 26 °C, which is the limit in a typical office for acceptable comfort (Hoyt et al. 2013), attaining *TC* using NV as the only means of cooling is challenging. Thus, an additional system is required to maintain the occupants' *TC*, while consuming minimal energy. One of the most studied systems for energy savings and comfort is personalized ventilation (PV) (Fanger 2000). PV units provide each occupant with the possibility to

E-mail: farah@aub.edu.lb

List of symbols

dT_{facial}/dt	rate of change of facial temperature (°C/min)	N	total number of iterations
dT_{indoor}/dt	rate of change of indoor temperature (°C/min)	PID	proportional integral derivative
e_k	temperature difference between T_{facial} and $T_{facial\text{-}set}$ of this iteration	PV	personalized ventilation
		Q_{SPV}	personalized ventilator supply flow rate (L/s)
e_{k-1}	temperature difference between $(T_{facial})_k$ and $T_{facial\text{-}set}$ of the previous iteration	RH	relative humidity (%)
		TC	thermal comfort
e_{k-2}	temperature difference between $(T_{facial})_k$ and $T_{facial\text{-}set}$ of the 2 previous iterations	T_{facial}	facial temperature (°C)
		T_{indoor}	indoor temperature (°C)
$\sum_{i=0}^{k} e_i$	integral error	TMY	Typical Meteorological Year
		T_{SPV}	personalized ventilator supply temperature (°C)
HVAC	heating, ventilation and air conditioning	$(T_{SPV})_k$	feedback value of present T_{SPV} (°C)
IES-VE	Integrated Environmental Solutions-Virtual Environment	τ	process time constant (min)
		τ_i	integral time (min)
K	process gain	τ_d	derivative time (min)
K_c	proportional gain	τ_c	IMC control time constant (min)
NV	natural ventilation	θ	time delay (min)

generate and control one's own preferred microenvironment (Melikov 2004). Recent studies have integrated mechanical cooling, NV with PV, and concluded that such integrated systems saved energy while still maintaining the occupants' comfort levels (Taheri et al. 2016; Khalil et al. 2020). However, spaces conditioned by only NV-PV systems are subject to airflow and temperature transients that cause variation in *TC* levels of a seated individual during occupancy hours (Khalil et al. 2020). Thus, the individual may have to perform recurrent and continuous changes to the PV's operational settings (temperature and/or flow rate) to meet own comfort needs, which is not practical as this affects working performance (Mishra et al. 2016). Hence, an adaptive NV-PV controller should automatically adjust the PV settings whenever there is discomfort while also minimizing the intervention of the occupant.

The design of an adaptive NV-PV controller primarily requires identification of the PV unit's control parameters. PV's individual control is one of its most essential features where occupants have full control of different parameters such as direction, airflow rate (Q_{SPV}) and PV supply temperature (T_{SPV}) (Lipczyńska 2015). However, such a solution would complicate the installation as well as the usage of the system in practical applications (Lipczyńska 2015). Experimental human subject results revealed that changing the Q_{SPV} avoided possible discomfort while consuming less energy compared to controlling the T_{SPV} (Lipczyńska 2015). Consequently and in most of the PV applications, the occupant controls Q_{SPV} while maintaining a constant T_{SPV} (Melikov et al. 2002; Melikov 2004; Veselý and Zeiler 2014; Taheri et al. 2016). The majority of previous studies in this field utilized PV systems in office spaces or test chambers that were maintained under constant indoor conditions by means of mechanical cooling systems up to 28 °C (Alsaad and Voelker 2020; Xu et al. 2020). However, keeping T_{SPV} constant might fail in providing *TC* at an elevated indoor temperature (T_{indoor}) as well as transients in T_{indoor} and relative humidity (RH) originating from NV (Zhang 2003). Thus and in such situations, changing both T_{SPV} and Q_{SPV} is important to avoid any possible discomfort situation. Moreover, minimal discomfort is vital with other forms of transients that occur due to changes in the occupant's metabolic rate (activity level) from walking for example, before sitting at the desk. Allowing the occupant to control simultaneously the two PV supply variables might not bring the needed *TC* at the same rate versus when the person is controlling a single operational variable, especially in transient conditions. The occupant can quickly notice a change in a single variable, such as changing Q_{SPV} from 0 L/s to 15 L/s, as adopted in many previous studies (Melikov 2004; Melikov et al. 2013; Taheri et al. 2016). For example, at low T_{SPV}, the occupant might favor relatively low Q_{SPV} over high Q_{SPV}, while at high T_{SPV} the occupant preference would be reversed. This direct relation between changing the supply Q_{SPV} and occupant *TC* at fixed T_{SPV} may become more complex and will require from the occupant to manipulate the PV operating conditions several times before reaching a *TC* state. Therefore, for NV spaces conditioned with PV, an adaptive controller varies one variable, $T_{SPV,}$ while still allowing the occupant to change Q_{SPV} as desired.

Moreover, estimating *TC* is critical for the success of the automated NV-PV system. *TC* prediction by means of

steady *TC* models such as PMV is not accurate and will not be applicable in spaces conditioned by NV-PV systems due to presence of transients with NV (De Dear and Brager 2002). Thus, *TC* prediction in NV-PV spaces needs a more appropriate correlation or model. The correlation should account for non-uniformity in the environment around the person due to PV operation and for thermal transients induced by NV as well as changes in occupant metabolism. Since different individuals have different thermal sensations under the same environmental conditions (Humphreys and Nicol 2002), the correlation must rely on influential segmental physiological parameters to predict *TC* (Shan et al. 2020). Physiological parameters, mainly segmental skin temperatures, demonstrated a good correlation with *TC* (González-Alonso 2012). The body segments used in *TC* prediction should be of limited number and must not be covered to allow for the measurement of corresponding skin temperatures using non-invasive and non-contact devices that do not affect the occupant's daily activities. Recent reviews revealed several non-invasive or mini-invasive, non-contact methods that can be used to measure skin temperatures (Warthmann et al. 2019; Andre et al. 2020; Yang et al. 2020). Non-invasive methods involve video and imaging, such as the use of infrared cameras integrated with face and pose tracking systems (Metzmacher et al. 2018). This method can be used to monitor human thermal physiological signals with errors varying between ±0.06 °C (during steady conditions) and ±0.99 °C (during transient cooling conditions) when compared with conventional contact sensors (Yang et al. 2020). Another system with promising accuracy includes the use of normal cameras of computers or cell phones integrated with Euler video magnification method and personalized skin sensitivity index (Cheng et al. 2017; Cheng et al. 2019). The average error with this method can be as low as 0.26 °C (Cheng et al. 2019). On the other hand, an accurate method that is mini-invasive involves using wearable accessories like eyeglasses integrated with infrared sensors of accuracy reaching ±0.1 °C as those used for medical applications (Ghahramani et al. 2018). The infrared sensors extract the skin temperature from the desired spots on the face such as cheeks, nose and ears and then were used with a hidden Markov model-based learning method (Ghahramani et al. 2018). Recent studies utilized thermographic cameras as means to measure skin temperatures and consequently applied them in *TC* modeling (Burzo et al. 2014; Cosma and Simha 2018). These studies proved that the average face temperature was highly correlated to the occupants' *TC* levels. Along with facial skin temperature, present research studies suggest associating *TC* with indoor environmental parameters (T_{indoor} and *RH*) (Daum et al. 2011). The *TC* correlation should be able to predict *TC* when transients in indoor conditions exist. Thus, combining environmental parameters as well as segmental skin temperatures of accessible body parts are essential in developing a *TC* model to predict correctly the occupant's comfort state.

Recently, the study of Itani et al. (2021) revealed a multivariable linear regression method for the development of an accurate correlation to predict *TC* as a function of occupant physiological and environmental parameters. They deduced and validated a *TC* correlation for a space that relies on the hybrid NV-PV cooling system for an average occupant's characteristics. This correlation expresses *TC* in terms of facial temperature (T_{facial}), T_{indoor}, *RH*, and the rate of change of T_{facial}, dT_{facial}/dt, applicable under steady or transient conditions. The regression correlation was developed using a validated bioheat model (Al-Othmani et al. 2008; Karaki et al. 2013) and a *TC* model (Zhang 2003) in steady and transient thermal states and room conditions. The correlation was applicable for NV spaces with T_{indoor} ranging between 25 and 33 °C, *RH* between 55% and 80%, and metabolic rate between 1 and 2 met (58 and 116 W/m^2). Since the reported *TC* correlation did not account for individual differences like gender, age, weight, height, acclimatization, and body composition, it is important to allow for individual control of Q_{SPV}, along with the adaptive T_{SPV} control, to account for such individual variations. Although many researches have tackled the design of an effective PV system for providing *TC*, none developed a robust model-based adaptive control methodology based on a mathematical *TC* correlation that takes into consideration the facial temperature and its rate of change with the environmental conditions to maintain *TC* in the presence of NV.

The current study aims to develop an autonomously controlled standalone PV unit to provide comfort in a NV office space with T_{indoor} that ranges between 25 and 33 °C, and *RH* between 55% and 80%. The adaptive NV-PV controller's design is to adjust robustly T_{SPV} at the occupant set Q_{SPV} and the current indoor environmental conditions, whenever there exists an uncomfortable thermal state. The controller sets T_{SPV} based on the measured T_{facial} and predicted *TC* using the adopted regression equation of Itani et al. (2021). A case study of an office space with moderate hot and humid indoor conditions implements the proposed controller within the constraints and applicability of the adopted correlation. The transient profile of T_{indoor} and *RH* of the NV-office space are determined using the building energy simulation software, IES-VE (ISE 2020). The developed adaptive controller is tested and its performance is evaluated in terms of attaining *TC* by using direct simulations on the bioheat model (Al-Othmani et al. 2008; Karaki et al. 2013) and *TC* model (Zhang 2003) for the tested cases.

2 Problem statement

This study considers a naturally ventilated office space equipped with PV unit. Accordingly, outdoor conditions as well as internal loads affect both T_{indoor} and RH. The office's desk has installed the controlled PV unit with its flow directed towards the seated occupant's upper body part as shown in Figure 1. The PV system delivers 100% conditioned fresh air towards the upper body segments including the trunk and the face. This allows for conditioning of air at the human body's proximity also known as the occupant's microclimate, thus improving TC (Yang and Clements-Croome 2012).

Since there might be situations with large temperature variations due to NV, the PV unit controller decides on the T_{SPV} that can attain a target T_{facial}, thus minimizing discomfort without causing thermal drafts. At the given T_{SPV} set by the controller, the occupant decides on Q_{SPV} while achieving personal comfort preference. Besides indoor transients, transients from changes in the metabolic rate of the occupant are also considered.

The overall TC level that the controller should maintain is between **0 (neutral)** and **1 (slightly comfortable)** based on Zhang's TC scale (Zhang 2003). These bounds are adopted since they reflect acceptable overall TC levels with relatively low energy consumption. Accordingly, a target T_{facial} can be obtained from a target overall TC level.

The controller takes four measured variables as input parameters proven influential in TC evaluation: T_{indoor}, RH, T_{facial} and dT_{facial}/dt. These measured parameters can predict the TC level based on the adopted regression equation (Itani et al. 2021) as defined in Eq. (1).

$$TC = -0.1325 \times T_{indoor}(^{\circ}\mathrm{C}) - 0.0004 \times RH(\%) - 1.0806 \times T_{facial}(^{\circ}\mathrm{C}) + 6.1386 \times \frac{\mathrm{d}T_{facial}}{\mathrm{d}t}(^{\circ}\mathrm{C}/\mathrm{min}) + 41.8240 \quad (1)$$

The above correlation was developed by Itani et al. (2021) using a validated bioheat model (Al-Othmani et al. 2008; Karaki et al. 2013) and a TC model (Zhang 2003) in steady and transient thermal states and room conditions. The developed correlation was also benchmarked with published experimental data of Pavlin et al. (2017) and Aryal and Becerik-Gerber (2019). The results showed good accuracy as reported in details by Itani et al. (2021). The adopted correlation applies to a range of T_{indoor} and RH between 25 and 33 °C, and 55% and 80%, respectively. These ranges are commonly encountered indoors for naturally ventilated spaces in the Mediterranean climate as well as the warm and humid climate of southern India (Doctor-Pingel et al. 2019; Khalil et al. 2020). If comfort is not attained, the controller then adjusts T_{SPV} and its rate of change under steady and transient conditions to attain a target T_{facial} that allows for maintaining TC between the acceptable bounds of 0 and 1 at the occupant set Q_{SPV}. The occupant has control over Q_{SPV} that could vary from 0 to 15 L/s (Kaczmarczyk et al. 2004; Schiavon and Melikov 2009), which could reflect the thermal preference of the occupant, while the range of T_{SPV} set by the controller is between 22 and 26 °C (Boerstra et al. 2014). A change induced by the occupant in Q_{SPV} would affect TC prediction. This is why, a single target TC value to be attained by the controller was not adopted, but rather an acceptable range of TC between 0 and 1. For example, at T_{indoor} of 30 °C, RH of 55%, T_{SPV} of 24 °C and steady conditions, varying Q_{SPV} from 0 L/s, 7 L/s, 10 L/s, and then to 15 L/s induced a TC level of −1.14 (slightly uncomfortable), 0.50 (just comfortable), 0.71 (between just comfortable and slightly comfortable) and 0.97 (slightly comfortable), respectively. Since the PV controller changes T_{SPV} to reach a target T_{facial} and attain TC there is a necessity to check whether the adopted TC correlation is sensitive to changes in T_{SPV}. Appendix A, which is in the Electronic Supplementary Material of the online version of this paper, examines the applicability of the adopted TC correlation (Itani et al. 2021) to transient situations with variable T_{SPV}.

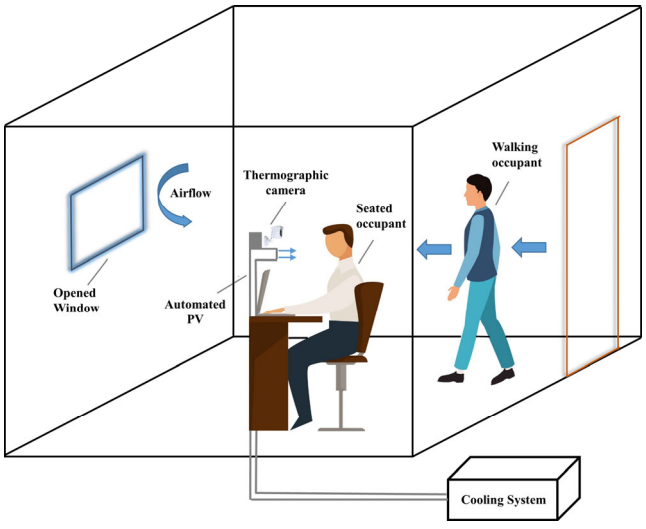

Fig. 1 Schematics of an automated PV unit with thermal imaging in a NV office space

The adopted TC correlation depends on the availability of fast high accuracy non-invasive or mini-invasive methods to record T_{facial} including any change that T_{facial} could experience with time. Assuming a calibrated thermal camera or an infrared sensor with an accuracy of ±0.1 °C is available (Ghahramani et al. 2018; Metzmacher et al. 2018; Cheng et al. 2019; Ryms et al. 2021), the effect on TC prediction would fall within a maximum error of ±0.75 on Zhang's TC scale from −4 (intolerable) to +4 (best comfort) (Zhang 2003). Accordingly, a thermal camera with improved

accuracy takes thermal videos rather than a single frame image and can process T_{facial} and dT_{facial}/dt every minute (Li et al. 2018). Moreover, accurate temperature and *RH* sensors can record indoor conditions every minute.

3 Methodology

The following subsections will present the proposed methodology for developing an adaptive NV-PV controller. To decide on an optimal design for the NV-PV controller, several factors are considered. Since the occupant has individual control of Q_{SPV} with the controller set to respond to different indoor environmental conditions, the design of the controller should take into consideration the three changing parameters Q_{SPV}, T_{indoor}, and *RH*. Hence, the data of T_{facial} and dT_{facial}/dt at different metabolic rates, indoor conditions (T_{indoor} and *RH*) and PV supply conditions help develop the adaptive controller's process transfer functions. To account for the nonlinearity in the process a multi-model approach will generate the transfer functions under various operating conditions. The Internal Model Control method (IMC) is then used to design the proportional-integral-derivative (PID) controller (Fruehauf et al. 1994). Subsequently, is the presentation of the developed strategy for controlling T_{SPV}. For practical PV application, an adoption of a feasible minimal change in T_{SPV} capable of inducing a change in *TC* is important. Moreover, a feasible minimal time for the controller to take action and change T_{SPV} is considered. This time should be relatively substantial to allow for the occupant thermal response, mainly T_{facial}, to vary upon a change in T_{SPV}. On the other hand, the time should be small enough to ensure a fast attainment of *TC*, especially during situations of high transients in metabolic rate that could extend over a period of 20 minutes (Zhu et al. 2003; Pavlin et al. 2017).

The developed controller with its adaptive design parameters is ultimately implemented in test cases of a NV office space, considering real life scenarios simulated on the bioheat model. The IES-VE software predicts indoor conditions with proper internal loads and external ambient conditions, as shown in the flowchart for the developed methodology in Figure 2. These indoor conditions need to be in the applicability range of the adopted *TC* correlation. The Q_{SPV} that the occupant can control varies continuously between 0 and 15 L/s as commonly used in previous studies (Kaczmarczyk et al. 2004; Schiavon and Melikov 2009; Keblawi et al 2011), while the range of T_{SPV} set by the controller is between 22 and 26 °C (Keblawi et al 2011; Boerstra et al. 2014). Comparison of simulated *TC* levels with the predicted ones from the adopted correlation using the bioheat and Zhang's *TC* models ensure that the NV-PV controller is working well.

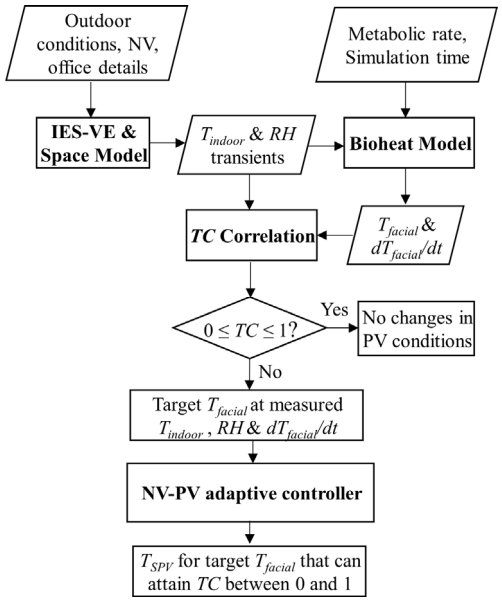

Fig. 2 Flow chart of the developed methodology

3.1 IES-VE model

The transient T_{indoor} and *RH* in the office space under study (presented in Section 4) are found using the IES-VE whole building simulation software (IES 2020). The bioheat model requires indoor conditions as input parameters (Al-Othmani et al. 2008; Karaki et al. 2013). Previous studies extensively used this software for predicting internal space temperature, electrical energy consumption, and for testing the suggested implementation of cooling control strategies of hybrid systems, including NV (Annan et al. 2016; Khalil et al. 2020; Mawson and Hughes 2020). IES-VE takes as input the layout of the studied space, the construction material, the internal loads with their operation schedule, and the weather and solar data of the selected region.

3.2 Bioheat and Zhang's *TC* models

A robust and a previously validated bioheat model (Al-Othmani et al. 2008; Karaki et al. 2013) can check for the applicability of the adopted *TC* correlation and for testing the controller in realistic transient case study scenarios. This model takes as input the metabolic rate, the environmental conditions, and the clothing criteria while outputting the skin temperature for 13 body segments (forehead, cheeks, backhead, chest, back, abdomen, upper arm, lower arm, palm, fingers, thigh, calf and foot) as well as the core temperature (Al-Othmani et al. 2008; Karaki et al. 2013). Figure 3(a) shows a schematic of the multi-segmented human body with its main segments. Care should be taken to input the segmental convective heat transfer coefficients and local microclimate air temperatures, especially those

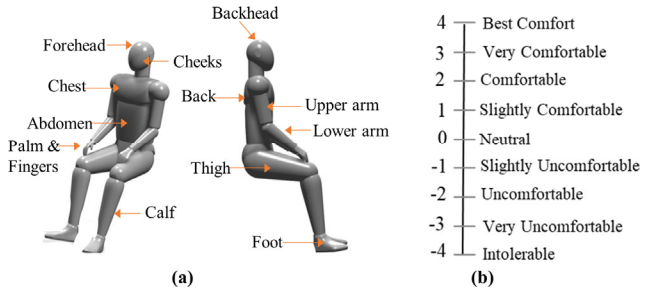

Fig. 3 Schematic showing the (a) multi-segmented bioheat model, and (b) *TC* scale (Zhang 2003)

affected by the PV operation, as previously done by Itani et al. (2021). The model can then predict T_{facial} (average temperature of the forehead and cheeks) and dT_{facial}/dt during transients, used as inputs in the adopted *TC* correlation.

Zhang's *TC* model can predict *TC* states under transient and steady thermal conditions as well as situations with individual control over the air supply conditions (Zhang 2003). Therefore, this model can obtain the simulated comfort in comparison with the predicted one using the adopted correlation of Itani et al. (2021). Zhang performed intensive human subjects experiments to develop a *TC* 9-point scale that ranged from −4 (intolerable) to +4 (best comfort), as shown in Figure 3(b) (Zhang 2003). The segmental skin temperatures and their rate of change outputted from the bioheat model are taken as inputs into the comfort model of Zhang to output the simulated *TC* state.

3.3 Data-based development of process transfer functions

Process transfer functions are required to develop the adaptive IMC-based PID controller that responds to the occupant-set Q_{SPV} as well as the different indoor conditions (T_{indoor} and *RH*). Data of T_{facial} and dT_{facial}/dt collected for a sample of 18 simulations conducted using the bioheat model; result in these process transfer functions. These simulations cover different indoor conditions with a range between 25 and 33 °C for T_{indoor} and with a range between 55% and 80% for *RH* as well as different PV conditions (T_{SPV} and Q_{SPV}) under a set profile of metabolic rate ranging between 1 and 2 met. The metabolic rate, which indicates the activity level, is a function of the heart rate that depends on the oxygen consumption at different levels of physical exertion for a typical person (Barstow and Molé 1991). The sample data used to develop the process transfer functions does not cover the entire range of possible operational conditions. Therefore, this is tested in the coming sections for real case scenarios over a wide range of possible indoor conditions and transient T_{indoor} and *RH*.

The adopted scenarios in the simulations consider a person with an initial metabolic rate of 2 met and an uncomfortable thermal state entering a space with indoor conditions of T_{indoor} = 25 °C (or 29 °C, or 33 °C) and *RH* = 55% (or 65%). After entering the space, the occupant's metabolic rate decreases gradually to reach 1 met computed according to the activity level equation (Barstow and Molé 1991). The PV is set to initially operate at Q_{SPV} of 7 L/s (or 10 L/s or 15 L/s) and a T_{SPV} of 22 °C to improve *TC*. The T_{SPV} then changes according to an arbitrary profile shown in Figure 4, over a period of 100 minutes. A period of 20 min was adopted in order to allow skin temperatures to stabilize after any induced change in metabolic rate of T_{SPV}.

The changes in T_{SPV} induce changes in T_{facial}, as presented in Figure 5 for two of the considered sample cases under T_{indoor} = 29 and 33 °C with *RH* = 65%. T_{facial} profile shows the same trend under the two different T_{indoor} of 29 and 33 °C.

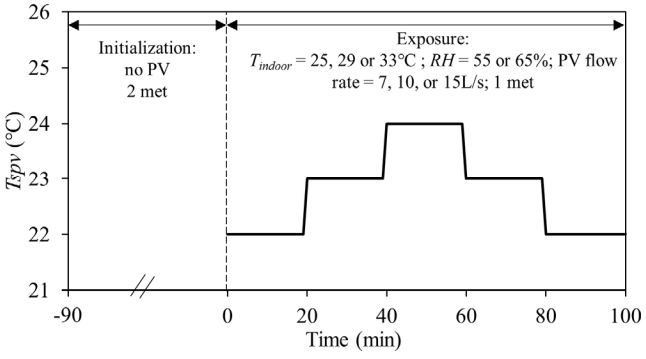

Fig. 4 Transient T_{SPV} profile under uniform indoor conditions for transfer functions development

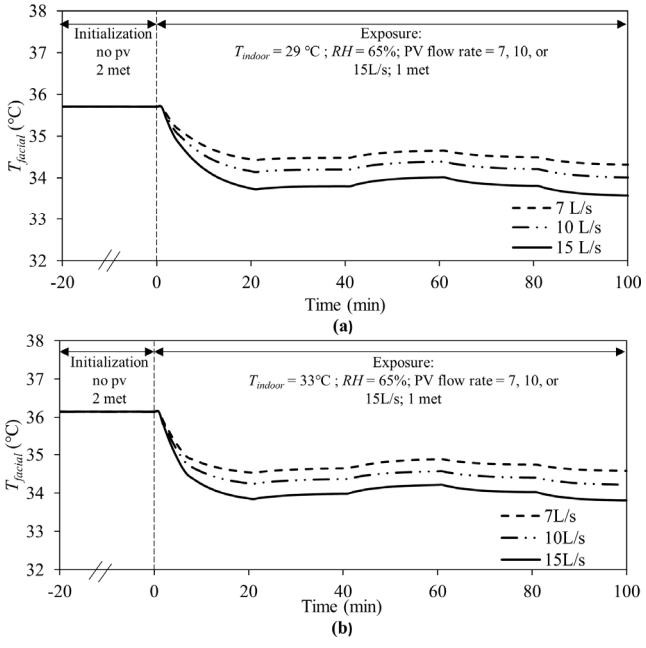

Fig. 5 Plots showing T_{facial} under (a) T_{indoor} = 29 °C and (b) T_{indoor} = 33 °C with *RH* = 65% for 3 different Q_{SPV} (7, 10 and 15 L/s)

T_{facial} starts with an initial value of 35.71 °C at T_{indoor} of 29 °C as shown in Figure 5(a), which is less than that of 36.15 °C at T_{indoor} of 33 °C as shown in Figure 5(b). T_{facial} increases gradually with increasing T_{SPV} from 22 to 24 °C for the first 60 minutes and then decreases with decreasing T_{SPV} from 24 to 22 °C for the remaining 40 minutes. As the flow rate increases from 7 to 15 L/s, T_{facial} decreases for both cases. Consequently, the resultant process transfer functions are deduced and presented in the results and discussion section. These process transfer functions will develop the adaptive IMC-based PID controller.

3.4 NV-PV adaptive controller development

Initially, there is the description of the temperature PID controller adopted in this study and the methodology followed for its parameter adjustments, followed by the presentation of the adaptive control strategy adopted for this application. Finally, the effect of two different incremental changes in T_{SPV} on *TC* is presented.

3.4.1 PID controller and its parameter adjustment

In this work, an adaptive model based temperature PID controller is designed to drive T_{facial} to its target value computed at the measured indoor environmental conditions and dT_{facial}/dt, thus maintaining *TC* between the acceptable bounds of 0 and 1. PID controllers have been extensively used for temperature regulation and control due to their simple structure, easy implementation and robustness (Song et al. 2016; Zhang et al. 2018).

The PID controller executes for a total number of iterations, *N*. At each iteration of the algorithm, k∈[0, ..., *N*], the PID reads the feedback value of present T_{facial}, $(T_{facial})_k$, and computes the difference between $(T_{facial})_k$ and its target temperature, target T_{facial}, as shown in Figure 6. Computation of the target T_{facial} is done using the adopted *TC* correlation with a target *TC* of 0.5 at the instantaneously measured indoor environmental conditions as well as dT_{facial}/dt for every iteration. The difference between $(T_{facial})_k$ and (target $T_{facial})_k$ is called the error, e_k. The PID integral action takes into account the sum of all errors ($\sum_{i=0}^{k} e_i$). Finally, the PID computes the derivative action determined from the current error (i.e. e_k) and the previous errors (i.e. e_{k-1} and e_{k-2}) using the discrete equation form.

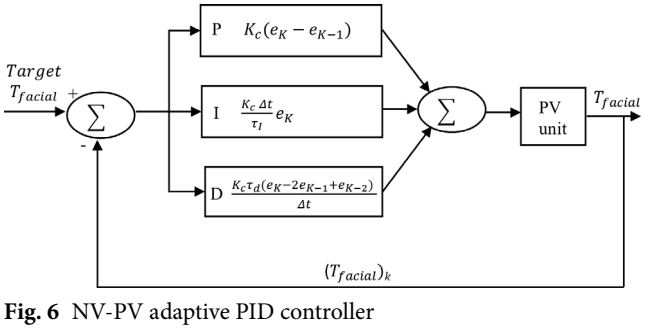

Fig. 6 NV-PV adaptive PID controller

The sum of the PID actions is then used by the PV system to adjust T_{SPV} at the next iteration, $(T_{SPV})_{k+1}$, while receiving feedback value $(T_{facial})_k$. The target T_{facial} is kept constant, as long as there is no violation of the *TC* constraint.

K_c, τ_i, and τ_d are the proportional gain, integral time, and derivative time, respectively and in addition are the main control parameters of the PID controller. The correct determination of these values is a key design of control systems. After generating the transfer functions from the multi-model approach, the IMC method (Fruehauf et al. 1994) will determine these PID tuning parameters. For a given process transfer function, G_P is given by

$$G_P = \frac{Ke^{-\theta s}}{\tau S + 1} \tag{2}$$

The IMC (Fruehauf et al. 1994) PID tunings can be obtained from

$$\begin{aligned} K_c &= \frac{1}{K}\frac{\tau + \theta}{\theta + \tau_c} \\ \tau_i &= \tau + \theta \\ \tau_d &= \frac{\tau\theta}{\tau + \theta} \end{aligned} \tag{3}$$

where K, θ, τ, and τ_c are the process gain, time delay, process time constant, and the specified closed loop time constant, respectively.

3.4.2 NV-PV control strategy

The automated NV-PV adaptive controller changes T_{SPV} to meet a target T_{facial} thus maintaining *TC* level between its acceptable bounds. The PV can operate at a range of Q_{SPV} between 0 and 15 L/s and T_{SPV} between 22 and 26 °C (Melikov et al. 2002; Schiavon and Melikov 2009; Keblawi et al. 2011). For practical PV application, an adoption of a feasible minimal change in T_{SPV} of 0.5 °C is adopted. Moreover, a feasible minimal time of 5 minutes for the controller to take action and change T_{SPV} is considered (Zhu et al. 2003; Pavlin et al. 2017;). A smaller time was not adopted in order to allow the occupant's T_{facial} to respond to any change in T_{SPV} and adjust accordingly the *TC*. The controller computes the target T_{facial} every 5 minutes using the adopted *TC* correlation (Itani et al. 2021) while adjusting T_{SPV} at the occupant-set Q_{SPV} and current indoor conditions, whenever there is detection of an uncomfortable state as shown in Figure 7. A representation of the detailed control

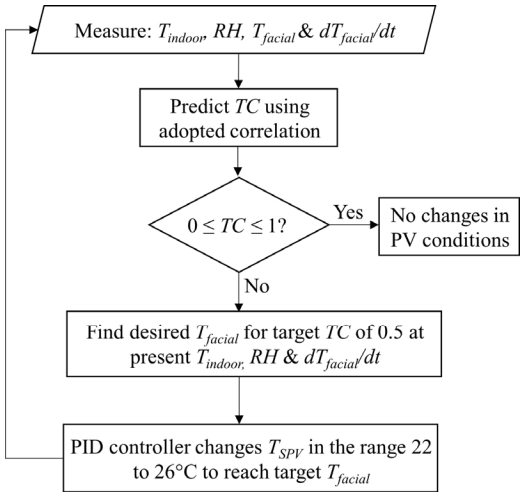

Fig. 7 NV-PV adaptive controller flowchart

strategy of the PV controller is as follows:

- Measurement of four input parameters each minute: T_{facial}, dT_{facial}/dt, T_{indoor}, and indoor RH.
- Prediction of TC using the adopted mathematical correlation (Itani et al. 2021).
- If the predicted TC falls between the acceptable range of 0 and 1, there is no control action needed otherwise calculation of a target T_{facial} that ensures a TC of 0.5, at the current indoor conditions, occurs using the adopted TC correlation (Itani et al. 2021).
- If the difference between the present T_{facial} and the target one is positive, a decrease in T_{facial} is necessary to reach the target value via decreasing T_{SPV} (depending on the difference between the present T_{facial} and the target value as discussed in Section 3.4.1) otherwise an increase in T_{SPV} should occur given that T_{SPV} ranges between 22 and 26 °C.
- Conducted simulations on the bioheat model showed a required minimum change of 0.5 °C in T_{SPV} to induce a significant change in TC as presented in Section 3.4.3. Thus, the PID controller computes T_{SPV} and takes action once the increment/decrement in T_{SPV} is not less than 0.5 °C. The T_{SPV} can vary every 5 minutes assuming a system response similar to that reported in previous studies (Deng and Missenden 1999; Zhu et al. 2003; Yao et al. 2013; Pavlin et al. 2017).

3.4.3 Effect of two different minimum incremental changes in T_{SPV} on TC

In order to decide on a feasible minimal increment in T_{SPV} while still attaining TC, considerations of the different factors affecting the system's performance are essential. Such factors include high transients initiated due to changes in metabolic rates or indoor conditions as well as situations where fast cooling is required. To this end, a test of two typical minimum incremental changes in T_{SPV} (0.5 °C and 1 °C) are needed to check the controller's ability in attaining TC during situations of high transients in T_{facial} at different indoor environmental conditions. The adopted minimum incremental changes should take into consideration the time needed to reach TC as well as the level of TC attained throughout the transient period until arriving at steady conditions.

Accordingly, the implementation of the comparison of TC results for three cases simulated on the bioheat model consider a person with an initial metabolic rate of 2 met and an uncomfortable thermal state entering a space with indoor conditions of T_{indoor} = 25 °C and RH = 60% (or 27 °C and RH = 70%, or 30 °C and RH = 70%). After entering the space, the occupant's metabolic rate decreases gradually to reach 1 met while the PV is initially operated at Q_{SPV} of 10 L/s (or 15 L/s at T_{indoor} = 30 °C) and at T_{SPV} of 22 °C to improve TC. The controller then changes T_{SPV} every 5 minutes if needed to reach the target T_{facial} that ensures acceptable TC levels between 0 and 1 over a simulated period of one hour.

4 Case study for real-time implementation and testing of NV-PV adaptive controller

The space considered in this study is a typical office building with typical internal loads during the summer season. This study adopts the calibrated office space developed by Khalil et al. (2020), as shown in Figure 8 and is located in Beirut, Lebanon, with a total area of 240 m^2. The weather data are those of the Typical Meteorological Year (TMY) based on a period of 10 years extending from 2000 till 2009 (Khalil et al. 2020). The cooling control strategy followed in Khalil et al.'s work (2020) is adjusted based on the consideration of the fully open windows during the occupied hours without the aid of any mechanical cooling system. The detailed

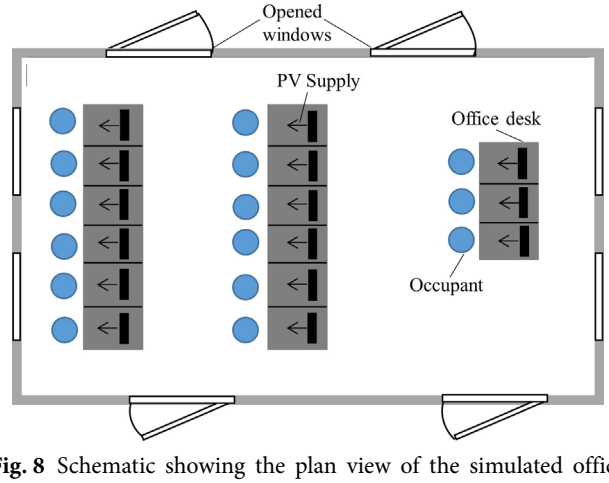

Fig. 8 Schematic showing the plan view of the simulated office space

description of the adopted office space is available in Khalil et al.'s study (2020).

Utilizing the validated bioheat model will ensure testing of the dynamic response of the NV-PV controller and its ability to maintain *TC* within the acceptable bounds instead of relying on human subject testing. Therefore, simulation case study scenarios that resemble real situations are conducted on the bioheat model. The case study scenarios consider transients in indoor conditions over a typical working schedule along with transients in the metabolic rate of a person arriving at 9 AM at the office and leaving for a one-hour break at noon. The person will then return to the office and leave at 6 PM. Table 1 shows the adopted transient profile in the metabolic rate over the working hours. Moreover, the scenarios consider a profile of the occupant-set Q_{SPV} over the whole working day as shown in Table 2. Simulations on IES-VE are conducted to find the transient indoor conditions (T_{indoor} and *RH*) for the representative days of June and August, which are typical hot and humid summer months (results shown in Section 5.3). Inputs to the bioheat model to predict T_{facial} and dT_{facial}/dt include these indoor conditions as well as the metabolic rate and Q_{SPV} profile. Moreover, inputs to the controller that would recommend T_{SPV} over the simulated time include the variables T_{indoor}, *RH*, T_{facial}, and dT_{facial}/dt. The target value of *TC* based on the recommended T_{SPV} should be between 0 and 1 during the entire simulation period to ensure good testing results of the controller. Furthermore, comparison of the predicted *TC* under the adopted correlation and the simulated one using Zhang's model (Zhang 2003) further illustrates the testing results.

Table 1 etabolic rate profile over the working hours adopted in each of the case studies

Time (hr)	Metabolic rate profile
9 AM	Metabolic rate drops from 2 met at the end of the pre-conditioning period to stabilize at 1 met after occupant gets seated
12 noon	Occupant leaves the office for a one-hour break
12–1 PM	Occupant is exposed to the same transient T_{indoor} and *RH* but at elevated metabolic rate of 2 met
1 PM	Metabolic rate drops from 2 met at the end of the break period to stabilize at 1 met after occupant gets seated

Table 2 Q_{SPV} profile over the working hours adopted in each of the case studies

Time (hr)	Q_{SPV} profile
9–11 AM	Q_{SPV} = 10 L/s
11–12 PM	Q_{SPV} = 15 L/s (since T_{indoor} starts getting relatively high)
12–1 PM	Q_{SPV} = 0 L/s (PV turned off during break)
1–4 PM	Q_{SPV} = 10 L/s
4–6 PM	Q_{SPV} = 7 L/s (since T_{indoor} starts decreasing to acceptable values)

5 Results and discussion

The process transfer functions are first generated after which the PID control parameters are determined using the IMC method. The presentation of the effect of two different incremental changes in T_{SPV} (0.5 and 1 °C) on *TC* will aid in selecting the incremental change in T_{SPV} that induces the best comfort. The performance of the NV-PV controller is then evaluated in case study scenarios on the basis of its success in maintaining acceptable *TC*. Finally, the applicability, limitations and future work related to the current work is presented.

5.1 Data-based development of process transfer function

Table 3 summarizes the coefficients of the process transfer functions relating T_{facial} to T_{SPV} under a sample of 10 operating conditions. Both T_{indoor} and *RH* showed a negative impact on the process gain and time constant, whereas increasing Q_{SPV} increased both *K* and τ. Based on the data in Table 3, the process gain can be obtained from

$$K = 0.9213 + 0.01808 \times Q_{SPV} - 0.0230 \times T_{indoor} - 0.00168 \times RH \quad (4)$$

with the process time constant estimated under all conditions using

$$\tau = 39.305 + 0.0485 \times Q_{SPV} - 1.017 \times T_{indoor} - 0.01974 \times RH \quad (5)$$

An average value for the time delay is adopted with

$$\theta = 0.782 \quad (6)$$

Table 3 Transfer function coefficients under a sample of 10 operating conditions

RH (%)	T_{indoor} (°C)	Q_{SPV} (L/s)	*K*	τ	θ
65	29	7	0.204	8.870	0.500
65	29	10	0.252	9.030	0.500
65	29	15	0.319	9.010	0.500
65	33	7	0.145	4.320	0.894
65	33	10	0.176	4.950	0.697
65	33	15	0.214	5.190	0.622
55	29	7	0.207	9.180	0.500
55	29	15	0.323	9.230	0.500
55	33	7	0.143	4.640	1.750
55	33	15	0.214	5.410	0.582

For any given operating conditions, the above equations determine the transfer function coefficients from which the IMC PID tunings are calculated. Successful testing of the nonlinear/adaptive PID tuning approach happens under different scenarios as described in subsequent sections.

5.2 Effect of two different minimum incremental changes of T_{SPV} on *TC* results

This section will present the evaluation results of the two different minimum incremental limits on T_{SPV} for the three different indoor conditions. Figure 9(a) and Figure 9(b) show the controller's changes in T_{SPV} every 5 minutes and the predicted *TC*, respectively. These changes are for the adopted 0.5 and 1 °C minimum increment in T_{SPV} under T_{indoor} = 25 °C, RH = 60%, and Q_{SPV} = 10 L/s. Similar results are also presented in Figure 10 and Figure 11 but for T_{indoor} = 27 °C and T_{indoor} = 30 °C, respectively.

In Figure 9(a) and during the first 10 minutes, the controller kept T_{SPV} constant at 22 °C. This is due to the operation of the controller for attaining the target *TC* as fast as possible. During this time, the metabolic rate is gradually dropping from 2 to 1 met and the face is being cooled, which involves high transients in T_{facial}. Upon reaching a *TC* of 1 (shown in Figure 9(b)), the controller increases T_{SPV} by a minimum increment of 0.5 °C or 1 °C every 5 minutes to maintain *TC* between the acceptable bounds of 0 and 1. During this time, the *TC* deviates between the two minimum incremental limits, where under the 0.5 °C increment *TC* is better. This can be justified since a lower T_{SPV} maintained for a longer time induces better comfort results. The *TC* profile for the 0.5 °C minimum increment

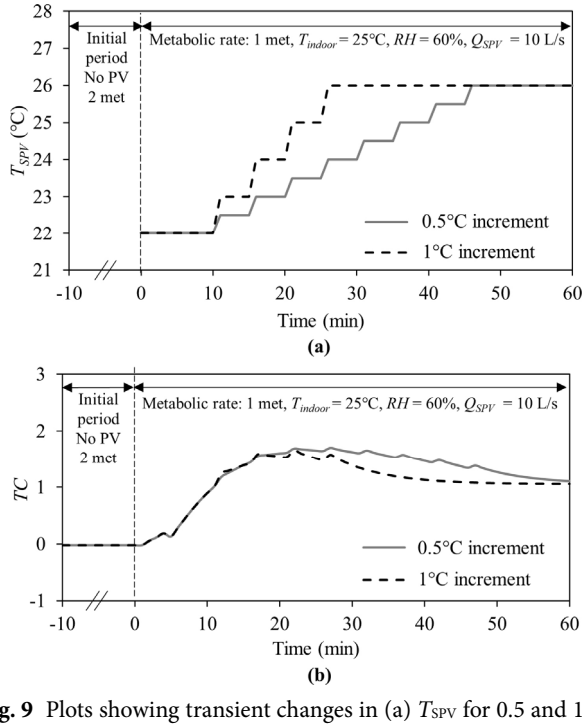

Fig. 9 Plots showing transient changes in (a) T_{SPV} for 0.5 and 1 °C increment and (b) *TC*, for T_{indoor} = 25 °C, RH = 60%, and Q_{SPV} = 10 L/s

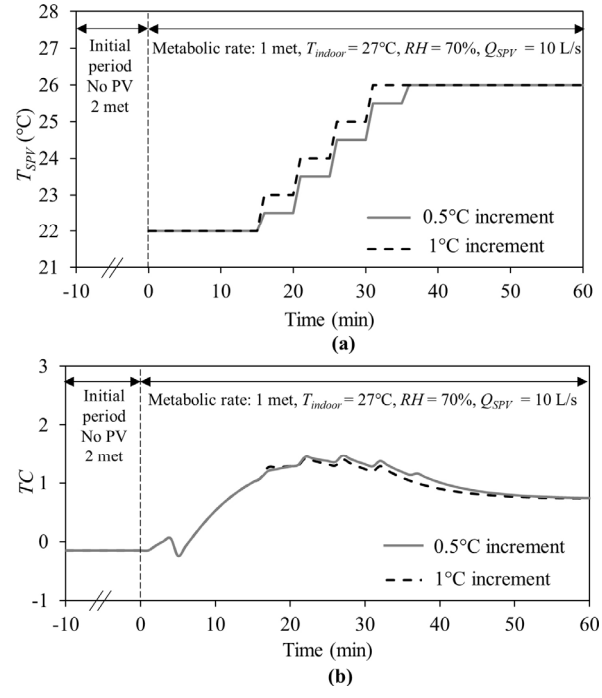

Fig. 10 Plots showing transient changes in (a) T_{SPV} for 0.5 and 1 °C increment and (b) *TC*, for T_{indoor} = 27 °C, RH = 70%, and Q_{SPV} = 10 L/s

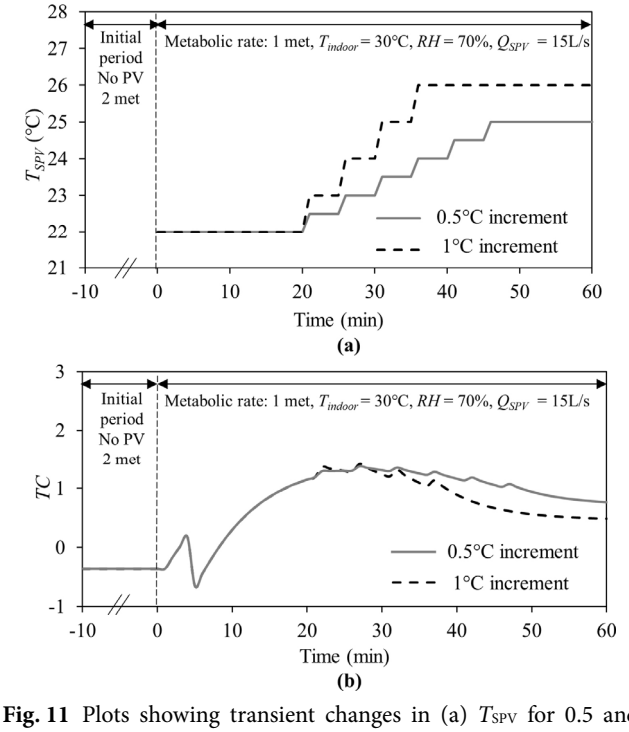

Fig. 11 Plots showing transient changes in (a) T_{SPV} for 0.5 and 1°C increment and (b) *TC*, for T_{indoor} = 30 °C and RH = 70%, and Q_{SPV} = 15 L/s

in T_{SPV} has more overshoots whenever a change in T_{SPV} occurs compared to the *TC* profile for the 1 °C increment. This is due to the more gradual changes in T_{SPV} for the 0.5 °C minimum increment compared to the 1 °C. Even though the 0.5 °C increment takes a longer time to reach a stabilized T_{SPV} value (about 45 minutes) than the 1 °C increment (about 25 min), the *TC* throughout the last 50 min for the 0.5 °C increment is better. Thus, the adoption of the 0.5 °C minimum increment is important in order to avoid any possibility in discomfort that could arise when an occupant intervenes to either increase or decrease Q_{SPV}. Similarly, the results discussed are found at the other simulated conditions shown in Figure 10 and Figure 11. However, the final steady state T_{SPV} value attained using the 0.5 °C and 1 °C increments deviated by about 1 °C in Figure 11. This is due to the fact that the controller does not trigger further changes in T_{SPV} when the predicted *TC* falls in the acceptable range between 0 and 1.

5.3 Case study evaluation results

Simulations of the study case scenarios' are conducted to test the dynamic response of the NV-PV controller and its success in maintaining a target *TC* between 0 and 1. Figure 12 shows the transient indoor conditions (T_{indoor} and *RH*) for the representative days of June and August as outputted from the IES-VE software.

Figure 13(a) shows the time variation in T_{SPV} as recommended by the NV-PV controller and the corresponding T_{facial} for a typical working day in the month of June. In addition, Figure 13(b) illustrates a comparison between the predicted and simulated *TC* over the working day. At 9:00 AM, the occupant enters the office space at a relatively high metabolic rate of 2 met feeling neutral ($TC = -0.01$) at a relatively low T_{indoor} of 25.08 °C with T_{facial} of 35.31 °C as shown in Figure 13. The adaptive controller automatically sets T_{SPV} to its minimum value of 22 °C at Q_{SPV} of 10 L/s causing a quick improvement in *TC* for the first two minutes as shown in Figure 13(b). Meanwhile, as the occupant sits, his/her metabolic rate starts decreasing gradually reaching 1 met and T_{facial} drops to reach 34.13 °C within 15 minutes, while *TC* reaches 1.6 (comfortable). Afterwards, the controller increases T_{SPV} with an increment of 1 °C per 5 minutes to reach 26 °C at 9:31 AM. After this time, *TC* starts dropping but is still above the 0 minimum, while T_{SPV} is fixed at 26 °C. At 11 AM, T_{indoor} reaches 28 °C and the occupant manually increases Q_{SPV} from 10 L/s to 15 L/s. This causes the *TC* to overshoot slightly to 0.99 after which it gradually decreases reaching 0.89 at noon, as shown in Figure 13(b). It is important to note that when the occupant increases Q_{SPV}, T_{SPV} maintains constant at 26 °C, which does not counteract the occupant preference for more cooling via increasing Q_{SPV}. At noon, the occupant leaves the office (metabolic rate gradually increases to 2 met) and comes back at 1 PM feeling slightly uncomfortable ($TC = -0.71$) at T_{indoor} of 30.26 °C with an elevated T_{facial} of 35.76 °C. The controller turns on the PV at a T_{SPV} of 22 °C and Q_{SPV} of 10 L/s keeping it constant for the next 30 minutes, while T_{facial} decreases to 34.05 °C and *TC* improves to 1.02. Subsequently, the NV-PV controller gradually increases T_{SPV} at an increment of 0.5°C to reach a value of 24.5 °C and preserve *TC* between 0 and 1 before 4 PM. With decreasing T_{indoor} reaching 29.4 °C, the occupant decreases Q_{SPV} from 10 L/s to 7 L/s at 4 PM. After that, the controller increases T_{SPV} to 25.5 °C (1 °C increment) and keeps it constant till the end of the working hours. Consequently, T_{facial} increases to reach a final value of 34.82 °C with a *TC* level of 1.05. Comparing the predicted *TC* to the simulated one, similar transient profiles are observed throughout the working

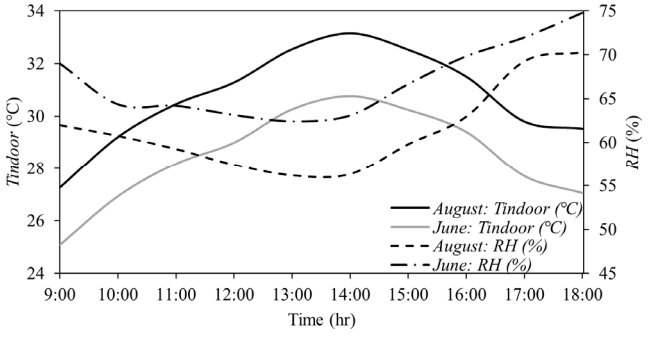

Fig. 12 Indoor conditions (T_{indoor} and *RH*) over the working hours for the months of June and August

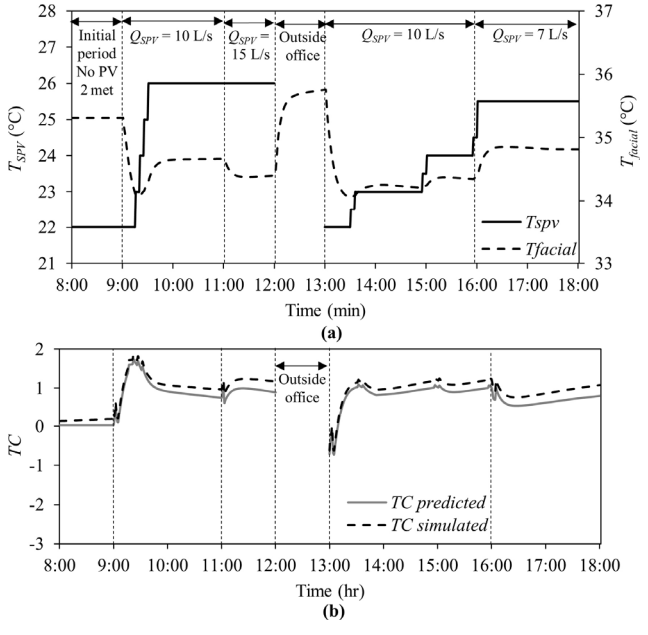

Fig. 13 Plots showing the transient variation in (a) T_{SPV} as well as T_{facial} and (b) the predicted *TC* compared to the simulated one for a typical working day of June

period with a maximum deviation of 0.2 as shown in Figure 13(b).

Similarly, for the month of August, Figure 14(a) and Figure 14(b) show the time variation in T_{SPV} as recommended by the NV-PV controller with the corresponding T_{facial}, and a comparison between the predicted and simulated *TC*, respectively. Since the occupant arrives at a relatively high metabolic rate feeling just uncomfortable (*TC* = −0.2) at T_{indoor} of 27.3 °C, the PV controller responds in a similar way as in June for the first 15 minutes. T_{SPV} starts with a minimum value of 22 °C (at Q_{SPV} of 10 L/s) and increases by 0.5 °C in the next 5 minutes reaching 22.5 °C till 9:20 AM and causing a drop in T_{facial} to 34.12 °C with an improvement in *TC* to 1.2 as shown in Figure 14(a) and Figure 14(b), respectively. The NV-PV controller then causes an increase in T_{SPV} at a rate of 1 °C per 5 minutes reaching a T_{SPV} of 25.5 °C at 9:31 AM causing an increase in T_{facial} to 34.3 °C and a slight drop in *TC* to 1. For the next 150 minutes, T_{SPV} is maintained at 25.5 °C even when the occupant increases Q_{SPV} to 15 L/s at 11 PM. This is due to the acceptable level of *TC* maintained between 0 and 1, while also reaching 0.54 at noon just before the occupant leaves the office. At 1 PM, the occupant comes back to the office feeling slightly uncomfortable (*TC* = −0.8) with a relatively high metabolic rate, T_{indoor} of 32.54 °C, and T_{facial} around 35.95 °C. The controller turns on the PV at a T_{SPV} of 22 °C and Q_{SPV} of 10 L/s, which remain constant for the next three hours decreasing T_{facial} to 34.06 °C and improving *TC* to almost 0.82. At 4 PM, the occupant decreases Q_{SPV} from 10 L/s to 7 L/s, however, due to the deceasing trend of T_{indoor} (see Figure 12) the controller increases T_{SPV} to 23 °C while keeping it constant for the remaining working hours. This resulted in a slight drop in *TC* followed by an increase as T_{indoor} decreases reaching a *TC* level of 0.74 with T_{facial} of 34.42 °C. The predicted *TC* showed similar values compared to the simulated *TC* throughout the working period with a maximum deviation of 0.2 as shown in Figure 14(b).

Overall, the PV controller succeeded in attaining a *TC* level between 0 and 1 during a typical working day for both summer months. The controller recommended T_{SPV} values affected by the presence of indoor transients due to variations in indoor environmental conditions (T_{indoor} and *RH*) and occupant metabolic rate. Moreover, the controller responded well even when the occupant intervened to change Q_{SPV} (either by increasing or decreasing). Consequently, implementation of the developed controller is possible under steady and transient situations for typical indoor conditions, metabolic rates and PV settings specific to this study. In addition, it is important to note that in real experimentation the results' accuracy depends on the accuracy of the tools used to take measurements of T_{facial}, T_{indoor} and *RH*. The

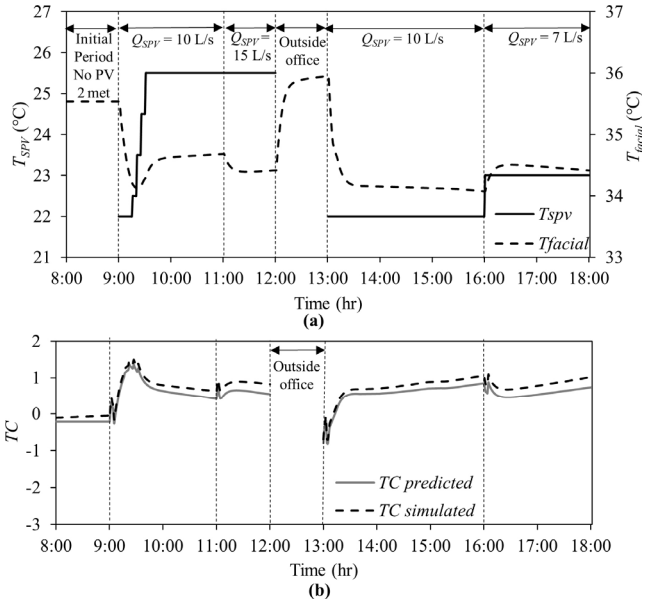

Fig. 14 Plots showing the transient variation in (a) T_{SPV} as well as T_{facial} and (b) the predicted *TC* compared to the simulated one for a typical working day of August

implementation of developed methodology for designing the current NV-PV controller can also be implemented with other PV unit designs as well as other *TC* correlations that might consider additional factors such as age, gender, and body composition.

5.4 Applicability, limitations and future work

The current study proposes an adaptive controller for the NV-PV system based on *TC* prediction using a previously developed correlation (Itani et al. 2021). Accordingly, the proposed system is applicable for T_{indoor} that ranges between 25 and 33 °C, *RH* between 55 and 80%, T_{SPV} between 22 and 26 °C, and Q_{SPV} between 0 and 15 L/s. Moreover, transient changes in metabolic rate between 1 and 2 met were accounted for in the proposed system. Within these temperature ranges and PV flow rate, the impact of the PV supply temperature on the room temperature is insignificant (Mousa et al. 2017). However, the indoor environment is assumed to be at uniform conditions with respect to temperature and relative humidity. Non-uniformity in the macroclimate due asymmetric radiation fields caused by longwave solar radiation effects in proximity to windows was neglected. The proposed system can overcome some of these assumptions, since the occupant has the privilege of controlling Q_{SPV} as desired.

It is important to note that the successful operation of the proposed controller depends on the accuracy of the measurement method of T_{facial}. In order to predict the occupant's *TC* using the adopted correlation of Itani et al.

(2021), the effect of the uncertainty in estimating *TC* should preferably be less than the change in *TC* when varying Q_{SPV} between 0 and 15 L/s. This would allow the occupant to offset the discomfort level that resulted from under or over estimation of *TC* due to measurement errors of T_{facial} and dT_{facial}/dt. Consequently, the infrared camera or other non-invasive or mini-invasive devices should have a high accuracy to measure T_{facial} and dT_{facial}/dt as well as the indoor temperature and relative humidity readings. However, the more significant terms in estimating the *TC* from the correlation are T_{facial} and dT_{facial}/dt. Thus, to have a *TC* variation of about ±1 on Zhang's *TC* scale, this dictates an accuracy of ±0.2 °C. This variation in *TC* can be decreased to ±0.75 on Zhang's *TC* scale if a device with accuracy of ±0.1 °C is used. In the market, the typical infrared camera accuracy is about ±2 °C (Cosma and Simha 2018; Li et al. 2018) where it can be improved when combined with calibration and face tracking methods (Cheng et al. 2017; Cheng et al. 2019; Metzmacher et al. 2018). Alternatively, and to overcome the issue of temperature accuracy, the infrared sensors of accuracy ±0.1 °C can be used (Ghahramani et al. 2018). This issue along with the radiation asymmetry effect in NV spaces can be investigated in future work. Moreover, human subject testing can be part of future work to validate the accuracy of the proposed approach in measuring T_{facial} and providing *TC* using the developed controller with minimal occupant interference.

6 Conclusions

Real time access to an occupant's dynamic *TC* allows the NV-PV system controllers to adjust continuously their operational settings while maintaining acceptable *TC* levels. Infrared thermography or other non-invasive devices can provide real time information about individuals' *TC* by constantly tracking T_{facial} and its rate of change, which proved to be strong indicators of *TC*. In this paper, the development of an autonomously controlled PV unit in a NV office space ensured an acceptable *TC* between 0 and 1 with T_{indoor} that ranged between 25 and 33 °C, and *RH* between 55 and 80%. A regression equation helped estimate *TC*. The adaptive NV-PV controller adjusted T_{SPV} based on the target T_{facial} that attained the desired *TC* deduced from the adopted mathematical correlation. The developed controller is implemented in a case study scenario of an office space in Beirut's moderate hot and humid climate with its performance evaluated in attaining *TC* using direct simulations of the bioheat and *TC* models. As shown, the developed controller achieves its goals in dynamically adjusting T_{SPV} and ensuring an acceptable *TC* of the occupant at all times of operation even with occupant intervention through changing the PV flow rate. The implementation of such autonomous PV units in office spaces is important for energy saving and ensuring *TC* for each occupant. The PV controller responds well under only a specific range of indoor temperatures and *RH,* as well as metabolic rates. This means that at more elevated indoor conditions and metabolic rates, establishment of a new regression model is required based on the new ranges. Future work may address the success of the system outside the considered range of this study along with experimental testing. Furthermore, addressing energy savings associated with the developed control over a full season of operation in comparison with conventional control methods of operation is paramount.

Acknowledgements

The authors would like to acknowledge the financial support of the University Research Board of the American University of Beirut grant award.

Electronic Supplementary Material (ESM): supplementary material is available in the online version of this article at https://doi.org/10.1007/s12273-021-0783-x.

References

Al Assaad D, Ghali K, Ghaddar N (2019). Effect of flow disturbance induced by walking on the performance of personalized ventilation coupled with mixing ventilation. *Building and Environment*, 160: 106217.

Al-Othmani M, Ghaddar N, Ghali K (2008). A multi-segmented human bioheat model for transient and asymmetric radiative environments. *International Journal of Heat and Mass Transfer*, 51: 5522–5533.

Alsaad H, Voelker C (2020). Qualitative evaluation of the flow supplied by personalized ventilation using schlieren imaging and thermography. *Building and Environment*, 167: 106450.

André M, de Vecchi R, Lamberts R (2020). User-centered environmental control: a review of current findings on personal conditioning systems and personal comfort models. *Energy and Buildings*, 222: 110011.

Annan G, Ghaddar N, Ghali K (2016). Natural ventilation in Beirut residential buildings for extended comfort hours. *International Journal of Sustainable Energy*, 35: 996–1013.

Aryal A, Becerik-Gerber B (2019). Skin temperature extraction using facial landmark detection and thermal imaging for comfort assessment. In: Proceedings of the 6th ACM International Conference on Systems for Energy-Efficient Buildings, Cities, and Transportation, New York, NY, USA

Barstow TJ, Molé PA (1991). Linear and nonlinear characteristics of oxygen uptake kinetics during heavy exercise. *Journal of Applied Physiology*, 71: 2099–2106.

Boerstra AC, Loomans MGLC, Hensen JLM (2014). Personal control over indoor climate and productivity. In: Proceedings of the 13th International Conference on Indoor Air Quality and Climate (Indoor Air 2014), Hong Kong, China.

Burzo M, Wicaksono C, Abouelenien M, et al. (2014). Multimodal sensing of thermal discomfort for adaptive energy saving in buildings. In: Proceedings of the Net Zero Symposium.

Cheng X, Yang B, Olofsson T, et al. (2017). A pilot study of online non-invasive measuring technology based on video magnification to determine skin temperature. *Building and Environment*, 121: 1–10.

Cheng X, Yang B, Tan K, et al. (2019). A contactless measuring method of skin temperature based on the skin sensitivity index and deep learning. *Applied Sciences*, 9: 1375.

Cosma AC, Simha R (2018). Thermal comfort modeling in transient conditions using real-time local body temperature extraction with a thermographic camera. *Building and Environment*, 143: 36–47.

Daum D, Haldi F, Morel N (2011). A personalized measure of thermal comfort for building controls. *Building and Environment*, 46: 3–11.

De Dear RJ, Brager GS (2002). Thermal comfort in naturally ventilated buildings: revisions to ASHRAE Standard 55. *Energy and Buildings*, 34: 549–561.

Deng S, Missenden JF (1999). Validation and simplification for a dynamic mathematical model of an air conditioning plant using classical control theory. *ASHRAE Transactions*, 105(1), 140–148

Doctor-Pingel M, Vardhan V, Manu S, et al. (2019). A study of indoor thermal parameters for naturally ventilated occupied buildings in the warm-humid climate of southern India. *Building and Environment*, 151: 1–14.

Fanger PO (2000). Indoor air quality in the 21st century: search for excellence. *Indoor Air*, 10: 68–73.

Feldmeier M, Paradiso JA (2010). Personalized HVAC control system. In: Proceedings 2010 Internet of Things (IOT), Tokyo, Japan.

Fruehauf PS, Chien IL, Lauritsen MD (1994). Simplified IMC-PID tuning rules. *ISA Transactions*, 33: 43–59.

Ghahramani A, Castro G, Karvigh SA, et al. (2018). Towards unsupervised learning of thermal comfort using infrared thermography. *Applied Energy*, 211: 41–49.

González-Alonso J (2012). Human thermoregulation and the cardiovascular system. *Experimental Physiology*, 97(3): 340–346.

Hoyt T, Schiavon S, Piccioli A, et al. (2013). CBE thermal comfort tool center for the built environment. University of California Berkeley. Available at http://comfort.cbe.berkeley.edu. Accessed 28 Sept 2020.

Huizenga C, Abbaszadeh S, Zagreus L, et al. (2006). Air quality and thermal comfort in office buildings: results of a large indoor environmental quality survey. In: Proceedings of Healthy Buildings 2006, 3, 393-397.

Humphreys MA, Nicol JF (2002). The validity of ISO-PMV for predicting comfort votes in every-day thermal environments. *Energy and Buildings*, 34: 667–684.

IES (2020). Introducing IESVE Software. Available at http://www. iesve. com/software.

Itani M, Ghaddar D, Ghaddar N, et al. (2021). Model-based multivariable regression model for thermal comfort in naturally ventilated spaces with personalized ventilation. *Journal of Building Performance Simulation*, 14: 78–93.

Jazizadeh F, Jung W (2018). Personalized thermal comfort inference using RGB video images for distributed HVAC control. *Applied Energy*, 220: 829–841.

Kaczmarczyk J, Melikov A, Fanger PO (2004). Human response to personalized ventilation and mixing ventilation. *Indoor Air*, 14: 17–29.

Karaki W, Ghaddar N, Ghali K, et al. (2013). Human thermal response with improved AVA modeling of the digits. *International Journal of Thermal Sciences*, 67: 41–52.

Keblawi A, Ghaddar N, Ghali K (2011). Model-based optimal supervisory control of chilled ceiling displacement ventilation system. *Energy and Buildings*, 43: 1359–1370.

Khalil S, Ghali K, Ghaddar N, et al. (2020). Hybrid mixed ventilation system aided with personalised ventilation to attain comfort and save energy. *International Journal of Sustainable Energy*, 39: 964–981.

Li D, Menassa CC, Kamat VR (2018). Non-intrusive interpretation of human thermal comfort through analysis of facial infrared thermography. *Energy and Buildings*, 176: 246–261.

Lipczyńska A (2015). Impact of combined system of personalized ventilation and chilled ceiling on indoor environment and energy consumption. PhD Thesis, Silesian University of Technology, Poland.

Mawson VJ, Hughes BR (2020). Deep learning techniques for energy forecasting and condition monitoring in the manufacturing sector. *Energy and Buildings*, 217: 109966.

Melikov AK, Cermak R, Majer M (2002). Personalized ventilation: evaluation of different air terminal devices. *Energy and Buildings*, 34: 829–836.

Melikov AK (2004). Personalized ventilation. *Indoor Air*, 14: 157–167.

Melikov AK, Skwarczynski MA, Kaczmarczyk J, et al. (2013). Use of personalized ventilation for improving health, comfort, and performance at high room temperature and humidity. *Indoor Air*, 23: 250–263.

Metzmacher H, Wölki D, Schmidt C, et al. (2018). Real-time human skin temperature analysis using thermal image recognition for thermal comfort assessment. *Energy and Buildings*, 158: 1063–1078.

Mishra AK, Loomans MGLC, Hensen JLM (2016). Thermal comfort of heterogeneous and dynamic indoor conditions—An overview. *Building and Environment*, 109: 82–100.

Mousa WAY, Lang W, Auer T, et al. (2017). A pattern recognition approach for modeling the air change rates in naturally ventilated buildings from limited steady-state CFD simulations. *Energy and Buildings*, 155: 54–65.

Nomura M, Hiyama K (2017). A review: Natural ventilation performance of office buildings in Japan. *Renewable and Sustainable Energy Reviews*, 74: 746–754.

Pavlin B, Pernigotto G, Cappelletti F, et al. (2017). Real-time monitoring of occupants' thermal comfort through infrared imaging: A preliminary study. *Buildings*, 7: 10.

Pérez-Lombard L, Ortiz J, Pout C (2008). A review on buildings energy consumption information. *Energy and Buildings*, 40: 394–398.

Ryms M, Tesch K, Lewandowski WM (2021). The use of thermal imaging camera to estimate velocity profiles based on temperature distribution in a free convection boundary layer. *International Journal of Heat and Mass Transfer*, 165: 120686.

Schiavon S, Melikov AK (2009). Energy-saving strategies with personalized ventilation in cold climates. *Energy and Buildings*, 41: 543–550.

Shan C, Hu J, Wu J, et al. (2020). Towards non-intrusive and high accuracy prediction of personal thermal comfort using a few sensitive physiological parameters. *Energy and Buildings*, 207: 109594.

Song J, Cheng W, Xu Z, et al. (2016). Study on PID temperature control performance of a novel PTC material with room temperature Curie point. *International Journal of Heat and Mass Transfer*, 95: 1038–1046.

Taheri M, Schuss M, Fail A, et al. (2016). A performance assessment of an office space with displacement, personal, and natural ventilation systems. *Building Simulation*, 9: 89–100.

Veselý M, Zeiler W (2014). Personalized conditioning and its impact on thermal comfort and energy performance—A review. *Renewable and Sustainable Energy Reviews*, 34: 401–408.

Warthmann A, Wölki D, Metzmacher H, et al. (2019). Personal climatization systems—A review on existing and upcoming concepts. *Applied Sciences*, 9: 35.

Xu C, Wei X, Liu L, et al. (2020). Effects of personalized ventilation interventions on airborne infection risk and transmission between occupants. *Building and Environment*, 180: 107008.

Yang T, Clements-Croome DJ (2012). Natural ventilation in built environment. In: Loftness V, Haase D (eds), Sustainable Built Environments. New York: Springer.

Yang B, Li X, Hou Y, et al. (2020). Non-invasive (non-contact) measurements of human thermal physiology signals and thermal comfort/discomfort poses—A review. *Energy and Buildings*, 224: 110261.

Yao Y, Huang M, Chen J (2013). State-space model for dynamic behavior of vapor compression liquid chiller. *International Journal of Refrigeration*, 36: 2128–2147.

Zhang H (2003). Human thermal sensation and comfort in transient and non-uniform thermal environments. PhD Thesis, University of California, Berkeley, USA.

Zhang J, Li H, Ma K, et al. (2018). Design of PID temperature control system based on STM32. *IOP Conference Series: Materials Science and Engineering*, 322: 072020.

Zhu S, Kato S, Song D, et al. (2003). Study on the personal air-conditioning system considering human thermal adaptation. In: Proceedings of the 4th International Symposium on HVAC, Beijing, China.